Rapid Communications

Kagome bands disguised in a coloring-triangle lattice

Shunhong Zhang,[1,2] Meng Kang,[3,2] Huaqing Huang,[2] Wei Jiang,[2] Xiaojuan Ni,[2] Lei Kang,[4] Shunping Zhang,[3] Hongxing Xu,[3,*] Zheng Liu,[1,5,*] and Feng Liu[2,5,*]

[1]*Institute for Advanced Study, Tsinghua University, Beijing 100084, China*

[2]*Department of Materials Science and Engineering, University of Utah, Salt Lake City, Utah 84112, USA*

[3]*School of Physics and Technology, Center for Nanoscience and Nanotechnology, and Key Laboratory of Artificial Micro- and Nano-structures of Ministry of Education, Wuhan University, Wuhan 430072, China*

[4]*Beijing Computational Science Research Center, Beijing 100193, China*

[5]*Collaborative Innovation Center of Quantum Matter, Beijing 100084, China*

(Received 3 August 2018; published 18 March 2019)

The kagome bands hosting exotic quantum phases generally and understandably pertain only to a kagome lattice. This has severely hampered the research of kagome physics due to the lack of real kagome-lattice materials. Interestingly, we discover that a coloring-triangle (CT) lattice, named after color-triangle tiling, also hosts kagome bands. We demonstrate first theoretically the equivalency between the kagome and CT lattices, and then computationally in photonic (waveguide lattice) and electronic (Au overlayer on electride Ca_2N surface) systems by first-principles calculations. The theory can be generalized to even distorted kagome and CT lattices to exhibit *ideal* kagome bands. Our findings open an avenue to explore the alluding kagome physics.

DOI: 10.1103/PhysRevB.99.100404

Two-dimensional (2D) lattice band models have been intensively studied in the context of band structure and band topology because Bloch electrons in such models give rise to exotic quantum effects. In general, a given band structure, such as the so-called kagome band as displayed in Figs. 1(a) and 1(b), pertains *only* to a given type of lattice, namely, the kagome lattice [Fig. 1(c)] [1]. On the other hand, two Hermitian Hamiltonians are equivalent to each other by a unitary transformation, producing identical eigenspectra. However, this equivalency has rarely been demonstrated between two different types of lattice models which could both be physically accessible. In this Rapid Communication, surprisingly, we discover that a kind of triangular lattice, which we call coloring-triangle (CT) lattice, has the identical kagome band as that of a kagome lattice. We will first prove mathematically the equivalence between these two lattices, which is of fundamental interest to further our study of 2D lattice models, and then demonstrate the construction of a CT lattice in real photonic and electronic materials, which has significant implications to advance the field of materials discovery for kagome physics.

The kagome lattice is one of the most interesting lattices mainly because it exhibits two exotic quantum phenomena. First, spin frustration in a kagome lattice with d electrons leads to a quantum-spin-liquid (QSL) phase [2]. Second, the kagome band, arising from a kagome lattice with single-orbital hopping, consists of two Dirac bands and one flat band [1]; the former, as in graphene [3,4], supports massless Dirac fermions and integer quantum Hall effects [5], and the latter accommodates strongly correlated topological states such as fractional quantum Hall effect [6–8]. Unfortunately, real materials having a kagome lattice are very difficult to find. So far, only a handful of materials have been identified to support the QSL phase. In fact, the field of QSL has been staggering for a while because herbertsmithite was the only promising material candidate for QSL [9] until the recent discovery of several other candidates, such as Zn-barlowite [10,11] and $YbMgGaO_4$ (with a triangular lattice) [12]. We have seen that each spin lattice model plays an important role in advancing the field, to provide a blueprint to guide the exploration and discovery of realistic materials with desired magnetic properties. On the other hand, a number of 2D materials possessing the geometry of a kagome lattice have been theoretically studied to realize kagome bands [13–16]. However, to date, experimental confirmation of kagome bands has only been achieved in artificial photonic lattices [17], but remains illusive for real electronic materials. In this regard, our discovery of another 2D lattice, i.e., the CT lattice, to also host the kagome band will significantly expand our search for the alluding flat-band materials.

The kagome lattice is featured with the corner-sharing equilateral triangles, subject to the highest wallpaper symmetry group, *P6mm*. In contrast, the CT lattice we discover here has a lower wallpaper symmetry (plane group $P3_1m$). Its geometry can be mapped onto a triangle tiling by filling the triangles with different edges using distinct colors [Fig. 1(d)], which is the reason we term it the CT lattice. Geometrically, this pattern can be labeled as "121213," belonging to one class of the popular wallpaper tilling patterns made by coloring triangles (see Fig. S1 in the Supplemental Material for the nomenclature of triangle tiling [18]). Physically, it means that one modifies a triangular lattice by selectively blocking some nearest-neighbor (NN) hoppings in a $\sqrt{3} \times \sqrt{3}$ supercell of

*Authors to whom correspondence should be addressed: hxxu@whu.edu.cn, zheng-liu@tsinghua.edu.cn, and fliu@eng.utah.edu

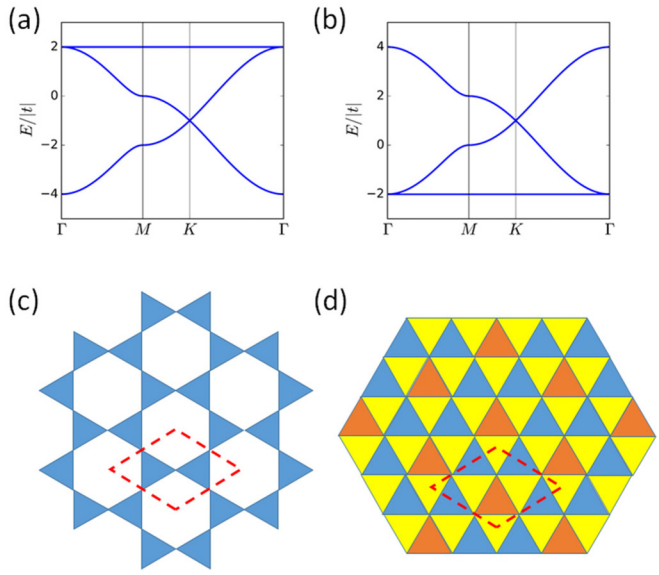

FIG. 1. Kagome bands along high-symmetry k paths, with (a) flat band on top and (b) flat band at bottom. The location of the flat band depends on the sign of the hopping integral. (c) The kagome lattice. (d) The CT lattice. The dashed red rhombus in (c) and (d) denotes the three-site unit cell.

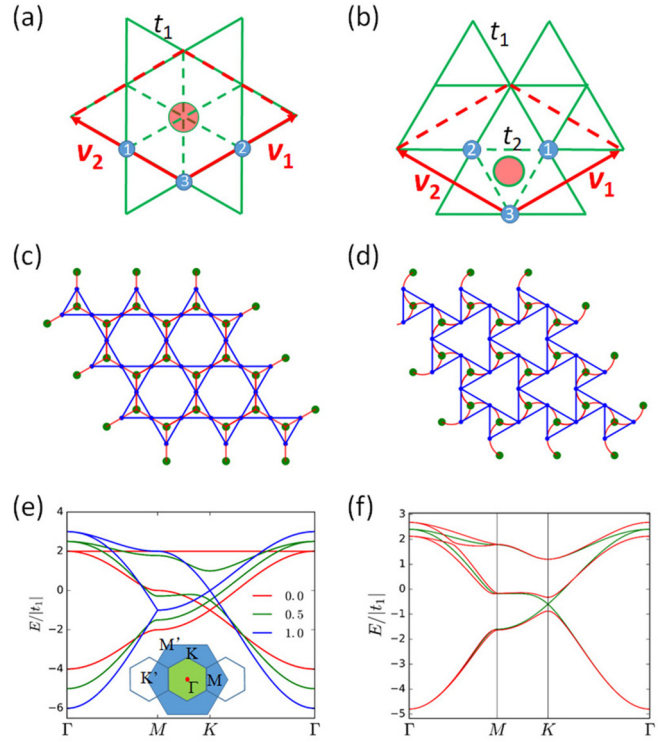

FIG. 2. Illustration of a (a) kagome lattice and (b) CT lattice formed by patterning a triangular lattice. The red arrows denote the patterned unit-cell basis vectors. (c) Line graph of a kagome lattice (blue) constructed from a parent hexagonal graph (lattice, green dots) with straight edges (red). (d) Line graph of a CT lattice (blue) constructed from a parent hexagonal graph (green dots) with curved edges (red). (e) Band variation in a $\sqrt{3} \times \sqrt{3}$ supercell of triangular lattice with one-third of the NN hoppings tuned from $t_2 = 0$ to $t_2 = t_1$ (bands corresponding to three typical t_2/t_1 ratios, namely, 0, 0.5, and 1, are presented). Note that for the $t_2 = 0$ case, the three bands are just folded from a single band of perfect triangular lattice. The inset shows the first Brillouin zone of the supercell (green) folded from that of the unit cell of the triangular lattice (blue). (f) The kagome bands realized in the CT lattice for $t_2 = t_1/4$, without (green) and with (red) SOC ($\lambda = 0.01t_1$).

a triangular lattice [see Fig. 2(b) and the discussion below]. Below we first prove that the CT lattice is equivalent to the renowned kagome lattice mathematically by a unitary transformation and line-graph construction [19–21].

We begin with the simplest triangular lattice of single-orbital hopping (the one that has mirror symmetry with respect to the lattice plane, such as s, p_z, or $d_z{}^2$). In this minimal model, each unit cell only contains one orbital and the Tight-Binding (TB) Hamiltonian in second quantization form reads

$$H = \sum_{\langle i,j \rangle} t_{ij} c_i^\dagger c_j + \text{H.c.}, \tag{1}$$

where $c_i^\dagger$ and c_j are the electron creation and annihilation operator at site i and j, respectively, with t_{ij} being the hopping integral. The summation runs only over all the NN sites. The triangular lattice can be patterned by altering the hoppings, which in turn forms interesting electronic bands. For example, in a previously studied dice or T_3 lattice [22], a patterned removal of one-third of NN hoppings leads to the emergence of localized electronic wave functions and hence flat bands. In fact, the kagome lattice shown in Fig. 1(c) can be realized by blocking the hoppings around one lattice site in a 2×2 supercell of triangular lattice, as illustrated in Fig. 2(a). In analogy, here we propose another patterning scheme by blocking the hoppings around the center of a triangle in a $\sqrt{3} \times \sqrt{3}$ supercell of a triangular lattice, as illustrated in Fig. 2(b). This results in the CT lattice, which physically can be realized by introducing a 2D periodic potential to make $t_2 = 0$ [Fig. 2(b)]. It can be shown that the NN hoppings in the CT lattice in Fig. 2(b) can be mapped to a trichromatic triangle tiling in Fig. 1(d) if one colors the triangles according to the hoppings along edges (bonds): blue for triangles with three unperturbed bonds (t_1), orange for triangles with three removed bonds ($t_2 = 0$), and yellow for the triangles with two t_1 and one t_2 bonds.

One can prove that the effective TB Hamiltonian associated with the CT lattice is equivalent to that of the conventional kagome lattice. The three-band Hamiltonian of the conventional kagome lattice can be expressed in the k space by a traceless matrix [1,6],

$$H^K(\vec{k}) = \begin{bmatrix} 0 & 2t_1 \cos(\vec{k} \cdot \vec{v}_3/2) & 2t_1 \cos(\vec{k} \cdot \vec{v}_1/2) \\ 2t_1 \cos(\vec{k} \cdot \vec{v}_3/2) & 0 & 2t_1 \cos(\vec{k} \cdot \vec{v}_2/2) \\ 2t_1 \cos(\vec{k} \cdot \vec{v}_1/2) & 2t_1 \cos(\vec{k} \cdot \vec{v}_2/2) & 0 \end{bmatrix}, \tag{2}$$

where $\vec{v}_3 = -(\vec{v}_1 + \vec{v}_2)$ is introduced for convenience. Diagonalization of this Hamiltonian gives rise to the kagome bands, which can be expressed as

$$E_0 = -2t_1; E_{\pm}(\vec{k}) = -t_1 \pm t_1\sqrt{8\cos(\vec{k}\cdot\vec{v}_1/2)\cos(\vec{k}\cdot\vec{v}_2/2)\cos(\vec{k}\cdot\vec{v}_3/2)+1}. \tag{3}$$

Correspondingly, the TB Hamiltonian of the CT lattice can also be constructed in k space as

$$H^{\mathrm{CT}}(\vec{k}) = \begin{bmatrix} 0 & t_1\left[e^{i\vec{k}\cdot\frac{\vec{v}_1-\vec{v}_3}{3}} + e^{i\vec{k}\cdot\frac{\vec{v}_3-\vec{v}_2}{3}}\right] & t_1\left[e^{-i\vec{k}\cdot\frac{\vec{v}_3-\vec{v}_2}{3}} + e^{-i\vec{k}\cdot\frac{\vec{v}_2-\vec{v}_1}{3}}\right] \\ t_1\left[e^{-i\vec{k}\cdot\frac{\vec{v}_1-\vec{v}_3}{3}} + e^{-i\vec{k}\cdot\frac{\vec{v}_3-\vec{v}_2}{3}}\right] & 0 & t_1\left[e^{i\vec{k}\cdot\frac{\vec{v}_2-\vec{v}_1}{3}} + e^{i\vec{k}\cdot\frac{\vec{v}_1-\vec{v}_3}{3}}\right] \\ t_1\left[e^{i\vec{k}\cdot\frac{\vec{v}_3-\vec{v}_2}{3}} + e^{i\vec{k}\cdot\frac{\vec{v}_2-\vec{v}_1}{3}}\right] & t_1\left[e^{-i\vec{k}\cdot\frac{\vec{v}_2-\vec{v}_1}{3}} + e^{-i\vec{k}\cdot\frac{\vec{v}_1-\vec{v}_3}{3}}\right] & 0 \end{bmatrix}. \tag{4}$$

A band structure identical to Eq. (3) can be obtained by diagonalizing Eq. (4). In fact, one can demonstrate that Eq. (4) is unitary transformable to (2) by using the following simple transformation matrix:

$$U = \begin{bmatrix} e^{-i\vec{k}\cdot\vec{v}_1/6} & 0 & 0 \\ 0 & e^{-i\vec{k}\cdot\vec{v}_2/6} & 0 \\ 0 & 0 & e^{-i\vec{k}\cdot\vec{v}_3/6} \end{bmatrix}. \tag{5}$$

Thus, the CT lattice is inherently equivalent to the kagome lattice. The physical connection between the U matrix elements and the movement of lattice sites is elucidated in Fig. S2 of the Supplemental Material [18]. One can further generalize our theory to a series of distorted lattices in between the kagome and CT lattices. In Eq. (5), we derived a transformation matrix with the diagonal elements containing a phase factor $\phi_l = \exp(-i\vec{k}\cdot\vec{v}_l/6)$ $(l = 1, 2, 3)$. This means that the unitary transformation represents a geometric operation between the kagome and CT lattice by rotating the two triangles inside the three-site unit cell about their center by an angle of $\theta = 30^\circ$. In such a rotation operation (note that it is not a pure rotation because the size/shape of the triangle also has to change slightly to fit the lattice), each site l in the kagome lattice moves by a vector of $-\vec{v}_l/6$ (which is the origin of the phase factor). Then, one can immediately see that another unitary matrix with a smaller rotation angle $(0 < \theta < 30^o)$ will also produce the same kagome band, except now $\phi_l = \exp(-i\sqrt{3}\tan\theta\vec{k}\cdot\vec{v}_l/6)$ (Fig. S2 of the Supplemental Material [18]). In principle, Eq. (5) can be extended to a more generic mathematic form by replacing the $v_l (l = 1, 2, 3)$ vectors with r_l which represents displacement of the lth lattice site (within the unit cell) from the original position of the kagome lattice. However, the hypothesis that all hopping integrals are equal is only physically plausible if all NN bonds have the same norm. This constraint then limits the possible deformations of the lattice to the CT-like pattern. This is very interesting because usually lattice distortion will inevitably modify the band structure. In contrast, we prove mathematically that for the types of distortions here, the band stays intact as these distortions represent a unitary lattice transformation. In fact, two previous calculations have indeed shown the kagome bands from such distorted lattices [15,16].

Furthermore, an elegant mathematical theory of line graph has been shown by Mielke in which the kagome lattice is in fact a line graph of hexagonal lattice which defines the condition for the existence of a flat band. Correspondingly, we found that the CT lattice as well as those distorted lattices in between the kagome and CT lattices are also line graphs of a hexagonal lattice as they should be, albeit with a different construction [illustrated in Figs. 2(c) and 2(d)] [18]. Consequently, all the exotic topological characteristics presented in kagome bands can also be achieved in the CT lattice. If one includes a nonvanishing t_2 and spin-orbit coupling or many-body interaction [23] in the CT lattice, it provides an extra degree of freedom to tune the band, as shown in Figs. 2(e) and 2(f) [18].

All the discussions above for electronic systems are readily transferrable to describe the dynamics of photonic systems [18,24]. Considering that there is a significant body of literature implementing flat-band models in a dielectric waveguide array [17], we first discuss how to realize a photonic CT lattice. We start by constructing a 2D photonic triangular lattice using silica (the refractive index $n_0 = 1.45$) as the bulk dielectric medium. The cylindrical waveguides distributed on the triangle lattice sites can be technically realized by the femtosecond direct-writing method [25]. Each waveguide supports one single mode, which is placed at a distance of 15 μm from each other to only allow for NN hopping, as determined by the interaction strength between adjacent waveguides. We set $\Delta n = 2.17 \times 10^{-3}$, the diameter of the waveguide is 4 μm, and the wavelength is 633 nm. The band structure was calculated using mode analysis in the full-wave numerical simulation software COMSOL 52a based on the finite-element method [26,27].

By removing a waveguide to block the hopping around it, one obtains the photonic kagome lattice [Fig. 3(a)]. The spacing is tuned to make next-nearest-neighbor (NNN) hopping negligible, so that an ideal photonic kagome band is obtained [Fig. 3(c)]. Each band is degenerate because of the high symmetry of the waveguide. To create a photonic CT lattice, the hopping term t_2 can be blocked by introducing air holes [28] which decrease the overlap of the evanescent wave [Fig. 3(b)]. When the air hole enlarges, the hopping term t_2 decreases. However, if it is too large, the symmetry of the field distribution will be broken and the band will split (Fig. S3 of the Supplemental Material [18]). Therefore, the air hole has to be delicately designed to match the field distribution so that t_2 can be reduced as much as possible while preserving the symmetry. After some attempts, we found a desired shape and size of air hole [Fig. 3(b)] to achieve the ideal kagome bands with a nearly flat band in the photonic CT lattice [Fig. 3(d)]. We note that the air hole can be replaced by a high refractive index waveguide [18], and hopping can be more delicately tuned by designing a chain of additional waveguides [18,29].

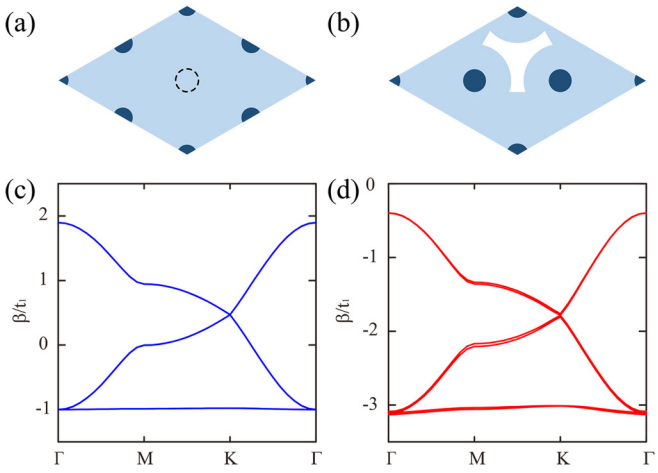

FIG. 3. Unit cell of photonic (a) kagome and (b) CT lattices formed by weakly coupled waveguide arrays (dark blue circles). The silica medium is colored light blue, and the air holes in the CT lattice are colored white. (c), (d) Band structure corresponding to the photonic kagome and CT lattices, respectively.

We expect that the photonic CT lattice we proposed above can be readily achieved experimentally in comparison with the photonic kagome lattice [30] to confirm our prediction. On the other hand, the realization of electronic materials of a CT lattice is more challenging. Nevertheless, below we demonstrate such a possibility based on an approach of patterning the nearly free 2D electron gas (2DEG). It has been theoretically proposed [31] that patterning 2DEG with a uniform triangular potential lattice can produce massless Dirac fermions. If one further tunes the triangular potential lattice based on the hopping texture of the CT lattice, in principle kagome bands should be present. Experimentally, scanning tunneling microscopy (STM) affords delicate manipulations of atoms or molecules on a clean crystal surface, making patterning of the surface electron gas practical [32]. In the search of nearly free 2DEG in realistic materials, we pay attention to electrides, a class of materials featured by the concept of "anionic excess electrons." In particular, we select monolayer Ca_2N, an experimentally already realized layered electride [33–36], as a candidate to materialize our patterning scheme.

Previous experimental and theoretical studies have shown the feasibility of Au to form a long-range ordered monolayer on different compound surfaces, which potentially realizes exotic electronic states [37–39]. In Ca_2N, the two layers of the interpenetrating Ca triangular lattice form a honeycomb lattice and, according to our first-principles calculations [40–43] (computational details can be found in the Supplemental Material [18]), the energetically favorable site for Au adsorption is the hollow site of the hexagons (on top of N atoms), as shown in Fig. 4(a).

In Fig. 4(b), we plot the 2D contour of charge density, before and after the deposition of an Au monolayer. One can clearly see that the top triangular lattice of Ca is patterned when the Au lattice is introduced, exhibiting a texture resembling our proposed CT lattice. The band structure of the Au patterned Ca_2N system in Fig. 4(c) displays a Dirac point at the first Brillouin zone corner, which we will show later is indeed a set of kagome bands originated from the CT lattice of Ca-*s* orbitals. The orbital composition of each band is denoted by the size of the circles. Due to the unique electride nature of Ca_2N, the bands near the Fermi level are occupied by electrons that are loosely bound to Ca ions, while the projected bands only count the charge in spheres around the ions but cannot fully capture the delocalized charge spreading out in real space. Therefore, Fig. 4(c) can only be viewed

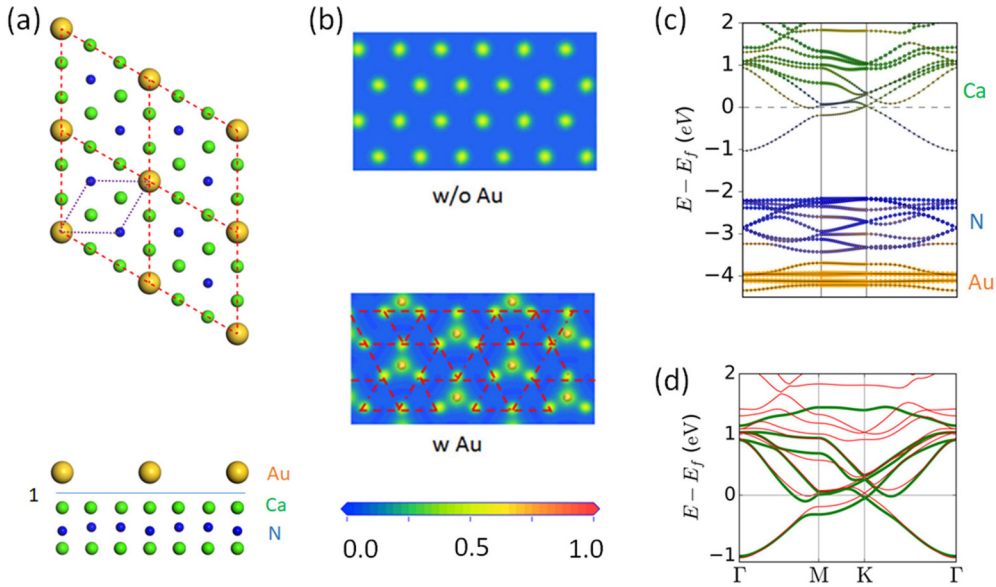

FIG. 4. (a) Top and side view of a triangular Au lattice deposited on the surface of a Ca_2N monolayer. The blue and red rhombus denotes the unit cell and $\sqrt{3} \times \sqrt{3}$ supercell of the pristine Ca_2N monolayer, respectively. (b) Charge density distribution in the plane 1 shown in the side view of (a), without and with the Au lattice patterning. (c) Electronic band structure of the Au-patterned Ca_2N monolayer, with band composition displayed in different colors. (d) The DFT band structure near the Fermi level (red) and the interpolated bands from MLWFs with Ca-*s* characteristics (green).

as a qualitative assignment of electronic bands into several manifolds according to the chemical species. However, by doing an electron counting, one can easily confirm that all N-p-orbital dominated bands are mainly distributed in an energy window ~2 eV below the Fermi level. On the other hand, it is clearly seen that the Au-5d6s bands are buried deep below the Fermi level. Considering the electronic configuration of Au atom ($5d^{10}\,6s^1$), one can conclude that each Au atom accommodates one extra electron from the underneath Ca_2N layer. Bader charge analysis confirms that ~0.97 electron is transferred from the Ca_2N monolayer to each Au atom, forming a triangular lattice of Au^- anions. The negative charge of Au^- anions is beneficial for its uniform distribution because the Coulomb repulsion can help prevent them from clustering on the Ca_2N surface similar to other surface overlayers [39].

Thus, the patterned system holds a nominal chemical formula $[Ca_2N]^+{}_3[e^-]_2[Au^-]$. The two excess anionic electrons with the smallest binding energy fill the highest occupied band, making the physics near the Fermi energy dominated by the kagome-like bands. They are separated from other occupied bands in energy, enabling us to study the low-energy physics by projecting them onto a subspace spanned by the Ca-s orbitals. Here we use the maximally localized Wannier functions (MLWFs) [44] as the basis instead of atomic s orbitals of Ca so as to include possible hybridization with other electronic states. Figure 4(d) shows that the bands formed by the MLWF basis well reproduce the salient features of density functional theory (DFT) bands, indicating the existence of two sets of kagome bands arising from the two layers of the patterned Ca-s triangular lattice, one on top right below the Au atoms and the other at the bottom farther away from Au [18].

Considering the relativistic effect of Au, spin-orbit coupling (SOC) may have a pronounced effect on the Ca-s dominated kagome bands. In Fig. S4(a) of the Supplemental Material [18], we plot the DFT band structure including SOC, where a gap of 106 meV at K is observed. However, a small electron pocket along the Γ-M path makes the bands not globally gapped, but only gapped at certain k points as in the topological electride Y_2C [45]. We find that by applying an in-plane biaxial strain, the electron pocket shrinks and finally disappears. The band evolution under a tensile strain is traced in Fig. S4(b) of the Supplemental Material [18]. The global gap emerges in a slightly strained structure ($<2\%$) and increases up to 40 meV as the strain is further raised to 8% [18]. We note that in-plane strain is a practical technique to tune the electronic structure and properties of 2D layered materials [46], and, more importantly, lattice engineering of Ca_2N has already been achieved in a recent experiment [47]. We further confirm the nontrivial band topology of the Au-decorated Ca_2N from first-principles calculations [48] and TB modeling [49] of the CT lattice with SOC [18].

Based on the above analysis, we summarize the roles of the Au triangular lattice in forming the topologically nontrivial kagome-like bands in the Au-Ca_2N system. (1) It provides a triangular periodic potential which patterns the nearly free 2DEG of the Ca_2N surface to create a CT lattice as our theoretical model predicts. (2) The stoichiometry (Ca_6N_3Au) and the electronic configuration of Au ($d^{10}s^1$) tune the Fermi level right at the Dirac points of the kagome-like bands. (3) The Au overlayer introduces strong SOC that opens a relatively large nontrivial band gap at the Dirac points. We have also tried the patterning procedure by using Ag or Cu instead of Au, which leads to a similar effect but with weaker SOC. The discovery of more and more new electride materials holding anionic electrons [50,51], especially the experimentally synthesized layered electrides such as Y_2C [45,52], provides a unique material platform to achieve the patterning procedure. The emergent 2D molecular crystals and metal-organic frameworks can serve as another category of candidates to materialize the proposed CT-lattice model.

In summary, we have rigorously proved the equivalency of a CT lattice to the conventional kagome lattice. Furthermore, we demonstrated the possibility to realize the CT lattice in both photonic and electronic systems. The well-developed femtosecond direct-writing method enables fabrication of an artificial photonic lattice with designer geometry and can be implemented to realize the photonic CT lattice. We suggest that layered electrides might provide a useful material platform for patterning 2DEG in order to realize a range of 2D lattices, including the CT lattice we propose here. It is worth mentioning that the idea of a CT lattice may be generalized to kagome magnetic [53] or cold-atom [54] systems.

Note added to proof. We would like to refer the readers to a recent paper [55] contributed by some of the authors of the present paper, which discussed the transition between two lattices (Lieb and kagome) with flat bands.

Work at Tsinghua University was supported by the Tsinghua University Initiative Scientific Research Program and the NSFC under Grant No. 11774196. Work at the University of Utah was supported by grants from the U.S. Department of Energy (DOE) (Grant No. DEFG02-04ER46148). Shunhong Zhang is supported by the National Postdoctoral Program for Innovative Talents of China (Grant No. BX201600091) and the Funding from China Postdoctoral Science Foundation (Grant No. 2017M610858). M.K., Shunping Zhang, and H.X. are thankful for the financial support from the National Key Basic Research Program (Grant No. 2015CB932400) and the National Natural Science Foundation of China (Grant No. 11674256). M.K. acknowledges financial support from the Wuhan University graduate student overseas exchange program. Numerical simulations of the photonic lattice were performed on supercomputers at Wuhan University. First-principles calculations were performed on the Tianhe-II supercomputer provided by The National Supercomputer Center in Guangzhou, China. The Paratera Tech Co. Ltd. is also sincerely acknowledged for the continuous technical support on high-performance computation.

[1] K. Ohgushi, S. Murakami, and N. Nagaosa, Phys. Rev. B **62**, R6065 (2000).
[2] L. Balents, Nature (London) **464**, 199 (2010).
[3] Y. Zhang, Y.-W. Tan, H. L. Stormer, and P. Kim, Nature (London) **438**, 201 (2005).
[4] C. L. Kane and E. J. Mele, Phys. Rev. Lett. **95**, 226801 (2005).

[5] H. M. Guo and M. Franz, Phys. Rev. B **80**, 113102 (2009).
[6] Z. Liu, F. Liu, and Y.-S. Wu, Chin. Phys. B **23**, 077308 (2014).
[7] Z. Liu, Z.-F. Wang, J.-W. Mei, Y.-S. Wu, and F. Liu, Phys. Rev. Lett. **110**, 106804 (2013).
[8] E. Tang, J.-W. Mei, and X.-G. Wen, Phys. Rev. Lett. **106**, 236802 (2011).
[9] M. R. Norman, Rev. Mod. Phys. **88**, 041002 (2016).
[10] Z. Liu, X. Zou, J.-W. Mei, and F. Liu, Phys. Rev. B **92**, 220102 (2015).
[11] Z. Feng, Z. Li, X. Meng, W. Yi, Y. Wei, J. Zhang, Y.-c. Wang, W. Jiang, Z. Liu, S. Li, F. Liu, J. Luo, S. Li, G.-q. Zheng, Z. Meng, J.-W. Mei, and Y. Shi, Chin. Phys. Lett. **34**, 077502 (2017).
[12] Y. Shen, Y.-D. Li, H. Wo, Y. Li, S. Shen, B. Pan, Q. Wang, H. C. Walker, P. Steffens, M. Boehm, Y. Hao, D. L. Quintero-Castro, L. W. Harriger, M. D. Frontzek, L. Hao, S. Meng, Q. Zhang, G. Chen, and J. Zhao, Nature (London) **540**, 559 (2016).
[13] Z. F. Wang, N. Su, and F. Liu, Nano Lett. **13**, 2842 (2013).
[14] B. Zhao, J. Zhang, W. Feng, Y. Yao, and Z. Yang, Phys. Rev. B **90**, 201403 (2014).
[15] X. Li, J. Zhou, Q. Wang, Y. Kawazoe, and P. Jena, J. Phys. Chem. Lett. **4**, 259 (2013).
[16] S. Kim, W. H. Han, I.-H. Lee, and K. J. Chang, Sci. Rep. **7**, 7279 (2017).
[17] D. Leykam, A. Andreanov, and S. Flach, Adv. Phys. X **3**, 1473052 (2018).
[18] See Supplemental Material at http://link.aps.org/supplemental/10.1103/PhysRevB.99.100404 for details.
[19] A. Mielke, J. Phys. A **24**, 3311 (1991).
[20] A. Mielke, J. Phys. A **24**, L73 (1991).
[21] A. Mielke, J. Phys. A **25**, 4335 (1992).
[22] B. Sutherland, Phys. Rev. B **34**, 5208 (1986).
[23] W. Zhu, S.-S. Gong, T.-S. Zeng, L. Fu, and D. N. Sheng, Phys. Rev. Lett. **117**, 096402 (2016).
[24] T. Ozawa, H. M. Price, A. Amo, N. Goldman, M. Hafezi, L. Lu, M. Rechtsman, D. Schuster, J. Simon, O. Zilberberg, and I. Carusotto, arXiv:1802.04173.
[25] S. Alexander and N. Stefan, J. Phys. B **43**, 163001 (2010).
[26] J.-M. Jin, *The Finite Element Method in Electromagnetics* (Wiley, New York, 2015).
[27] I. Andonegui and A. J. Garcia-Adeva, Opt. Express **21**, 4072 (2013).
[28] X. Ren, L. Feng, Z. Lin, and J. Feng, Opt. Lett. **38**, 1416 (2013).
[29] G. G. Pyrialakos, N. S. Nye, N. V. Kantartzis, and D. N. Christodoulides, Phys. Rev. Lett. **119**, 113901 (2017).
[30] Y. Zong, S. Xia, L. Tang, D. Song, Y. Hu, Y. Pei, J. Su, Y. Li, and Z. Chen, Opt. Express **24**, 8877 (2016).
[31] C.-H. Park and S. G. Louie, Nano Lett. **9**, 1793 (2009).
[32] M. R. Slot, T. S. Gardenier, P. H. Jacobse, G. C. P. van Miert, S. N. Kempkes, S. J. M. Zevenhuizen, C. M. Smith, D. Vanmaekelbergh, and I. Swart, Nat. Phys. **13**, 672 (2017).
[33] K. Lee, S. W. Kim, Y. Toda, S. Matsuishi, and H. Hosono, Nature (London) **494**, 336 (2013).
[34] D. L. Druffel, K. L. Kuntz, A. H. Woomer, F. M. Alcorn, J. Hu, C. L. Donley, and S. C. Warren, J. Am. Chem. Soc. **138**, 16089 (2016).
[35] J. S. Oh, C.-J. Kang, Y. J. Kim, S. Sinn, M. Han, Y. J. Chang, B.-G. Park, S. W. Kim, B. I. Min, H.-D. Kim, and T. W. Noh, J. Am. Chem. Soc. **138**, 2496 (2016).
[36] S. Zhao, Z. Li, and J. Yang, J. Am. Chem. Soc. **136**, 13313 (2014).
[37] Z. F. Wang, K.-H. Jin, and F. Liu, Nat. Commun. **7**, 12746 (2016).
[38] F.-C. Chuang, C.-H. Hsu, H.-L. Chou, C. P. Crisostomo, Z.-Q. Huang, S.-Y. Wu, C.-C. Kuo, Wang-Chi V. Yeh, H. Lin, and A. Bansil, Phys. Rev. B **93**, 035429 (2016).
[39] M. Zhou, W. Ming, Z. Liu, Z. Wang, P. Li, and F. Liu, Proc. Natl. Acad. Sci. **111**, 14378 (2014).
[40] H. J. Monkhorst and J. D. Pack, Phys. Rev. B **13**, 5188 (1976).
[41] P. E. Blöchl, Phys. Rev. B **50**, 17953 (1994).
[42] G. Kresse and J. Furthmüller, Phys. Rev. B **54**, 11169 (1996).
[43] J. P. Perdew, K. Burke, and M. Ernzerhof, Phys. Rev. Lett. **77**, 3865 (1996).
[44] N. Marzari, A. A. Mostofi, J. R. Yates, I. Souza, and D. Vanderbilt, Rev. Mod. Phys. **84**, 1419 (2012).
[45] H. Huang, K.-H. Jin, S. Zhang, and F. Liu, Nano Lett. **18**, 1972 (2018).
[46] C. Si, Z. Sun, and F. Liu, Nanoscale **8**, 3207 (2016).
[47] S. Kim, S. Song, J. Park, H. S. Yu, S. Cho, D. Kim, J. Baik, D.-H. Choe, K. J. Chang, Y. H. Lee, S. W. Kim, and H. Yang, Nano Lett. **17**, 3363 (2017).
[48] Y. Yao, L. Kleinman, A. H. MacDonald, J. Sinova, T. Jungwirth, D.-s. Wang, E. Wang, and Q. Niu, Phys. Rev. Lett. **92**, 037204 (2004).
[49] Y. Yang, Z. Xu, L. Sheng, B. Wang, D. Y. Xing, and D. N. Sheng, Phys. Rev. Lett. **107**, 066602 (2011).
[50] Y. Zhang, H. Wang, Y. Wang, L. Zhang, and Y. Ma, Phys. Rev. X **7**, 011017 (2017).
[51] W. Ming, M. Yoon, M.-H. Du, K. Lee, and S. W. Kim, J. Am. Chem. Soc. **138**, 15336 (2016).
[52] K. Horiba, R. Yukawa, T. Mitsuhashi, M. Kitamura, T. Inoshita, N. Hamada, S. Otani, N. Ohashi, S. Maki, J.-i. Yamaura, H. Hosono, Y. Murakami, and H. Kumigashira, Phys. Rev. B **96**, 045101 (2017).
[53] R. Chisnell, J. S. Helton, D. E. Freedman, D. K. Singh, R. I. Bewley, D. G. Nocera, and Y. S. Lee, Phys. Rev. Lett. **115**, 147201 (2015).
[54] N. Goldman, I. Satija, P. Nikolic, A. Bermudez, M. A. Martin-Delgado, M. Lewenstein, and I. B. Spielman, Phys. Rev. Lett. **105**, 255302 (2010).
[55] W. Jiang, M. Kang, H. Huang, H. Xu, T. Low, and F. Liu, Phys. Rev. B **99**, 125131 (2019).

Supplementary Materials for

Kagome Bands Disguised in a Coloring-Triangle Lattice: Theory and Materials

Shunhong Zhang[1,2], Meng Kang[3,2], Huaqing Huang[2], Wei Jiang[2], Xiaojuan Ni[2], Lei Kang[4], Shunping Zhang[3], Hongxing Xu[3], Zheng Liu[1,5] and Feng Liu[2,5]

[1]*Institute for Advanced Study, Tsinghua University, Beijing 100084, China*

[2]*Department of Materials Science and Engineering, University of Utah, Salt Lake City, Utah 84112, USA*

[3]*School of Physics and Technology, Center for Nanoscience and Nanotechnology, and Key Laboratory of Artificial Micro- and Nano-structures of Ministry of Education, Wuhan University, Wuhan 430072, China*

[4]*Beijing Computational Science Research Center, Beijing 100193, China*

[5]*Collaborative Innovation Center of Quantum Matter, Beijing 100084, China*

1. The coloring-triangle tiling

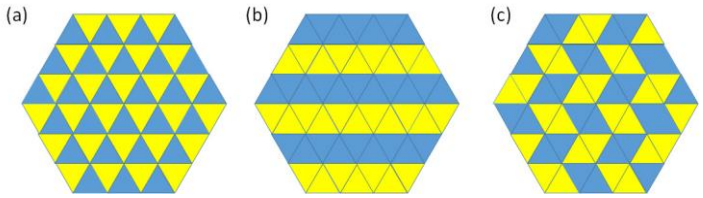

FIG. S1 Some typical coloring-triangle tiling patterns. (a) "121212", (b) "111222", and (c) "112122". For details see https://en.wikipedia.org/wiki/Triangular_tiling.

2. Transformation between the Kagome and CT lattice.

The generic form of a three-band model Hamiltonian reads

$$H(\vec{k}) = \begin{bmatrix} 0 & H_{12} & H_{31}^{*} \\ H_{12}^{*} & 0 & H_{23} \\ H_{31} & H_{23}^{*} & 0 \end{bmatrix} \quad (1)$$

The characteristic equation to diagonalize the Hamiltonian is

$$|\lambda I - H| = \lambda^3 + A\lambda + B = 0 \tag{2}$$

where $A(\vec{k}) = -(|H_{12}|^2 + |H_{23}|^2 + |H_{31}|^2)$ and $B(\vec{k}) = -2\,\mathrm{Re}(H_{12}H_{23}H_{31})$ are dependent on the momentum $\vec{k}$.

For the Kagome lattice, the tight-binding model with only the nearest neighbor hopping (t). The Hamiltonian elements can be expressed as

$$\begin{aligned} H_{12}^K &= t(e^{-i\vec{k}\cdot\vec{v}_3/2} + e^{i\vec{k}\cdot\vec{v}_3/2})e^{i\phi/3} = 2t\cos(\vec{k}\cdot\vec{v}_3/2)e^{i\phi/3} \\ H_{23}^K &= t(e^{-i\vec{k}\cdot\vec{v}_1/2} + e^{i\vec{k}\cdot\vec{v}_1/2})e^{i\phi/3} = 2t\cos(\vec{k}\cdot\vec{v}_1/2)e^{i\phi/3} \\ H_{31}^K &= t(e^{-i\vec{k}\cdot\vec{v}_2/2} + e^{i\vec{k}\cdot\vec{v}_2/2})e^{i\phi/3} = 2t\cos(\vec{k}\cdot\vec{v}_2/2)e^{i\phi/3} \end{aligned} \tag{3}$$

One can calculate the coefficients for the characteristic equation

$$\begin{aligned} A &= -4t^2[\cos^2(\vec{k}\cdot\vec{v}_1/2) + \cos^2(\vec{k}\cdot\vec{v}_2/2) + \cos^2(\vec{k}\cdot\vec{v}_3/2)] \\ B &= -16t^3\cos(\vec{k}\cdot\vec{v}_1/2)\cos(\vec{k}\cdot\vec{v}_2/2)\cos(\vec{k}\cdot\vec{v}_3/2)e^{i\phi} \end{aligned} \tag{4}$$

For simplicity we set the flux-related quantity $\phi = 0$. Considering the relationship $\vec{v}_1 + \vec{v}_2 + \vec{v}_3 = 0$, we have $-8t^3 - 2tA + B = 0$, i.e., Eq. (2) has a momentum-independent root $-2t$ which corresponds to a flat band, and the three bands can be expressed as follows:

$$E_0 = -2t; E_\pm = -t \pm t\sqrt{8\cos(\vec{k}\cdot\vec{v}_1/2)\cos(\vec{k}\cdot\vec{v}_2/2)\cos(\vec{k}\cdot\vec{v}_3/2)+1} \tag{5}$$

When a triangular lattice is patterned by a periodic potential so that some of the nearest neighbor hoppings are blocked as shown in FIG. 2(b) of the main text, the Hamiltonian elements of the CT lattice are

$$\begin{aligned} H_{12}^{CT} &= t[e^{i\vec{k}\cdot(\vec{v}_1-\vec{v}_3)/3} + e^{i\vec{k}\cdot(\vec{v}_3-\vec{v}_2)/3}] \\ H_{23}^{CT} &= t[e^{i\vec{k}\cdot(\vec{v}_2-\vec{v}_1)/3} + e^{i\vec{k}\cdot(\vec{v}_1-\vec{v}_3)/3}] \\ H_{31}^{CT} &= t[e^{i\vec{k}\cdot(\vec{v}_3-\vec{v}_2)/3} + e^{i\vec{k}\cdot(\vec{v}_2-\vec{v}_1)/3}] \end{aligned} \tag{6}$$

Considering the relationship $\vec{v}_1 + \vec{v}_2 + \vec{v}_3 = 0$, we have

$$\begin{aligned} H_{12}^{CT} &= 2t\cos(\vec{k}\cdot\vec{v}_3/2)e^{i\vec{k}\cdot(\vec{v}_1-\vec{v}_2)/6} \\ H_{23}^{CT} &= 2t\cos(\vec{k}\cdot\vec{v}_1/2)e^{i\vec{k}\cdot(\vec{v}_2-\vec{v}_3)/6} \\ H_{31}^{CT} &= 2t\cos(\vec{k}\cdot\vec{v}_2/2)e^{i\vec{k}\cdot(\vec{v}_3-\vec{v}_1)/6} \end{aligned} \tag{7}$$

Given that the lattice vectors are identical to the Kagome lattice, the form of A and B for the characteristic Eq. (2) turn out to be equal to those of the Kagome lattice. Therefore, the two lattices have exactly the same band diagrams. Indeed, the CT lattice can be converted into the conventional Kagome lattice via a unitary transformation:

$$H^K = UH^{CT}U^{-1} \tag{8}$$

with the unitary transformation matrix U appearing as Eq. (5) in the main text. The physical connection between the U matrix elements and the movement of lattice sites are elucidated in FIG. S2.

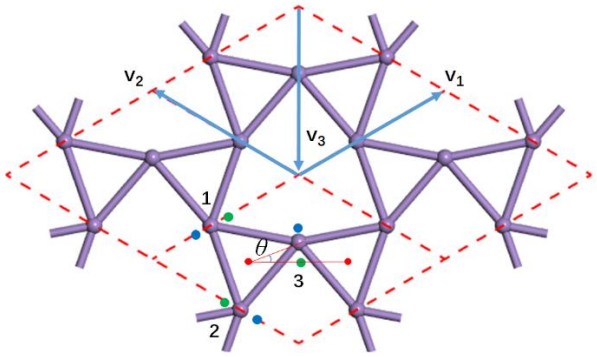

FIG. S2 Schematic illustration of evolution from the ideal Kagome lattice (θ=0°, green) to distorted ones (0°<θ<30°, purple), and finally to the CT lattice (θ=30°, blue). The site indexed l moves along the $\mathbf{v}_l$ vector, which contributes a phase factor to the TB Hamiltonian. The red circles denote the lattice sites of a honeycomb lattice based on which one can construct a line graph either in Kagome or CT geometry.

If one includes non-vanishing t_2 in the CT lattice, it provides extra degrees of freedom for the manipulation of the electronic structure. Essentially, the blocked NN hoppings t_2 in the CT lattice are similar to half of the next NN (NNN) hoppings in the conventional Kagome lattice (Note that standard Kagome lattice has six NNN hoppings in the unit cell, and t_2 in the CT lattice only captures three of them). FIG. 2(c) illustrates the band evolution in the CT lattice with a varying t_2/t_1 ratio. When this ratio goes from zero to one, the bands evolve from ideal Kagome bands to perturbed ones, and finally

recover to the folded triangular lattice bands, indicating a smooth connection between the CT and triangular lattices. The bottom and middle bands form Dirac points at K which are robust against the variation of t_2/t_1.

Next we demonstrate the equivalence between the photonic CT and Kagome lattice. We consider 2D photonic lattices composed of evanescently coupled waveguide arrays, as shown in FIG. 3(a) and (b) of the main text. The dynamics of a photonic lattice is described by the paraxial approximation for the diffraction of light propagation along weakly coupled waveguide array,

$$i\partial_z\psi(x,y,z) = -\frac{1}{2k_0}\nabla_\perp^2\psi(x,y,z) - \frac{k_0\Delta n}{n_0}\psi(x,y,z) \tag{9}$$

where ψ is defined by the envelop of electric field $\mathbf{E}(x,y,z) = \hat{\mathbf{e}}\psi(x,y,z)\exp(ik_0 z)$; $\hat{\mathbf{e}}$ is the unit vector in the direction of polarization and z is the light propagation direction; $\nabla_\perp^2 = \partial_x^2 + \partial_y^2$ acts on the transverse plane; $k_0=2\pi n_0/\lambda$ is the wavenumber in the bulk material with λ being the light wavelength; Δn is the deviation of refractive index of waveguide array from the bulk material that defines the photonic lattice. Compared with the Schrödinger equation of quantum mechanics, the propagation direction z plays the role of temporal coordinate, where the propagation of light along waveguide array is akin to the temporal derivative of quantum particle. The deviation of refractive index gives an external 2D periodic potential in the plane perpendicular to z direction. Band structure is given by the spectrum k_z (usually denoted as β) as a function of Bloch wave vector $\boldsymbol{k}_\perp=(k_x, k_y)$.

In a TB approximation, the evolution of wave amplitude propagating along each waveguide is described as [1,2],

$$i\partial_z\psi_{mn}(z) = \sum_{m',n'} t_1\psi_{m'n'}(z) \tag{10}$$

where $\psi_{mn}(z) = \varphi e^{i\beta z}e^{i\mathbf{k}_\perp\cdot(m\mathbf{v}_1+n\mathbf{v}_2)}$ is the amplitude of m, n-th waveguide in photonic lattice (defined by the real space lattice vectors $\mathbf{R}=m\mathbf{v}_1+n\mathbf{v}_2$); the summation runs over all NN waveguides. The hopping term (coupling strength) t_1 is determined by the

evanescent overlap between the transverse field distribution of the modes in adjacent waveguides. Interestingly, the three-band TB Hamiltonian of both the photonic Kagome and CT lattice turns out to be the same in *k*-space

$$H^K(\mathbf{k}) = H^{CT}(\mathbf{k}) = \begin{bmatrix} 0 & t_1(1+e^{-i\mathbf{k}_\perp\cdot\mathbf{v}_1}) & t_1(1+e^{-i\mathbf{k}_\perp\cdot\mathbf{v}_2}) \\ t_1(1+e^{i\mathbf{k}_\perp\cdot\mathbf{v}_1}) & 0 & t_1(e^{i\mathbf{k}_\perp\cdot\mathbf{v}_1}+e^{-i\mathbf{k}_\perp\cdot\mathbf{v}_2}) \\ t_1(1+e^{i\mathbf{k}_\perp\cdot\mathbf{v}_2}) & t_1(e^{-i\mathbf{k}_\perp\cdot\mathbf{v}_1}+e^{i\mathbf{k}_\perp\cdot\mathbf{v}_2}) & 0 \end{bmatrix} \quad (11).$$

Therefore, the photonic CT lattice of waveguide array is equivalent to Kagome lattice, which is indeed confirmed by our numerical simulations.

3. More details on realization of photonic CT lattice

The reduction of hopping term t_2 can be acquired by diminishing the interaction between adjacent waveguides. Air hole can be introduced to decrease the overlap of evanescent wave decaying away from waveguide. However, when it gets close to waveguide, the symmetry of mode distribution can be broken. An efficient solution to this dilemma is to match the air hole with field distribution as sketched in FIG. 3(b), so that the hopping t_2 can be blocked and meanwhile the symmetry broken is minuscule. Other similar shape of air hole can also work. For example, triangle air hole is used to achieve CT lattice [FIG. S3 (a) and (b)]. With the increasing size of triangle air hole, hopping term t_2 decreases and a nearly flat band arises [FIG. S3 (e) and (f)]. However, the symmetry is also destroyed, leading to significant band splitting and gap opening.

Another scheme to create a photonic CT lattice is introducing an extra array of waveguides with higher refractive index (Δn=0.014) and smaller diameter (2.35 μm) (black circle) in the triangular lattice, as shown in FIG. S3(c). Waveguides with high refractive index can bind light around it and decrease the hopping term t_2. But it's difficult to get exactly zero t_2 for high refractive index waveguide. High order modes appear with the increase of refractive index, which will increase hopping. Waveguides need to be contracted to only allow single mode propagation, which results in less bound of light and rise in hopping. It gives rise to a perturbed Kagome bands as shown in FIG. S3(g).

Photonic CT lattice is also achievable by flexibly tuning hopping by a chain of waveguide, as shown in FIG. S3(d). Triangular lattice with negligible NN hopping is

formed firstly in waveguide array (the distance of adjacent waveguides is added to be 30 μm). Additional waveguide chains are then inserted to increase NN hopping. By removing waveguide chains (dash circles) to block the hopping term t_2, CT lattice is finally obtained. The diameter and refractive index of waveguides are the same as those with air hole. The corresponding Kagome bands are shown in FIG. S3(h).

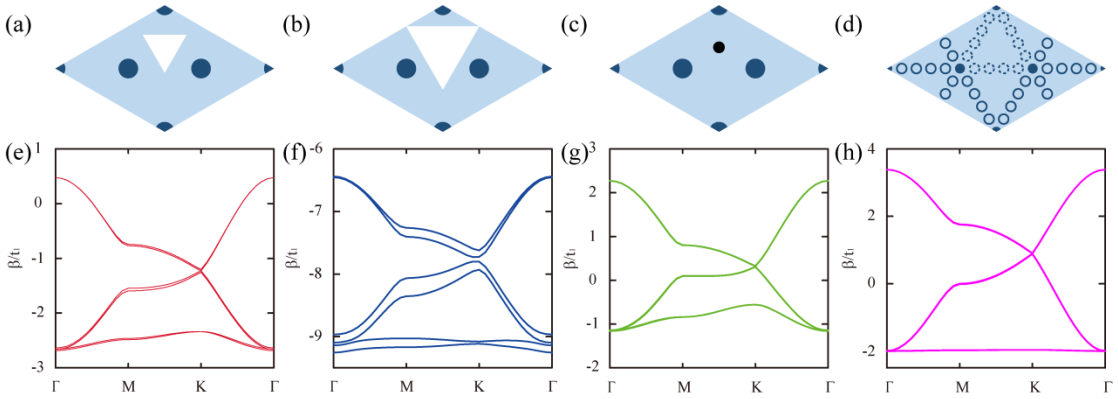

FIG. S3 Unit cell of photonic CT lattice created by introducing (a) and (b) triangle air holes (white triangle), (c) high refractive index waveguides (black circle), or (d) additional waveguide chains. (e)-(h) the corresponding band structure.

4. Computational details in DFT calculations

Using density functional theory (DFT) calculations, we studied the electronic structure of a triangular pattern of Au lattice deposited on a layered electride material, Ca_2N, as illustrated in FIG. 4(a) of the main text. The Vienna *Ab initio* simulation package (VASP) [3] is implemented for DFT calculations. Core-valance electronic interactions are treated by the projector augmented wave (PAW) [4] method and the energy cutoff for plane wave basis is 500 eV. The *k*-points in the Brillouin zone are sampled by the Monkhorst-Pack scheme [5]. Electron exchange-correlation interactions are treated by the PBE functional [6] with the Generalized Gradient Approximation (GGA). SOC is included in the electronic structure calculation. We have also examined the effect of van der Waals (vdW) interaction by relaxing the structure using the optB88-vdW functional, and no significant structural change was observed. Therefore, in the following, we report the results calculated by using the standard GGA-

PBE functional.

5. Band topology of the Ca_2N-Au system and strain engineering

The band structure of the Ca_2N-Au system with SOC is plotted in FIG. S4(a) and its evolution under biaxial strain is shown in FIG. S4(b). To characterize the band topology, we calculate the spin Berry curvature by using the Kubo formula [7]. The spin Berry curvature $\Omega^s(\boldsymbol{k})$ along high symmetric k-paths in FIG. S4(c) explicitly indicates that the system possesses topologically nontrivial bands, as characterized by the singularity at the K points. The spin Chern number of the system can be calculated by integrating the spin Berry curvature in the first BZ

$$C^s = \frac{1}{4\pi}\int_{BZ} d^2\vec{k}\Omega^s(\vec{k}) \tag{12}$$

which yields 1. This suggests that the system contain topologically nontrivial bands. Kagome bands are known to be inherently nontrivial. On the other hand, Ca_2N is topologically trivial. Therefore, by enforcing the Ca-4*s* orbitals of Ca_2N into a CT lattice, we effectively convert Ca_2N into a topological state, which might be suitable for realizing quantum spin Hall effect.

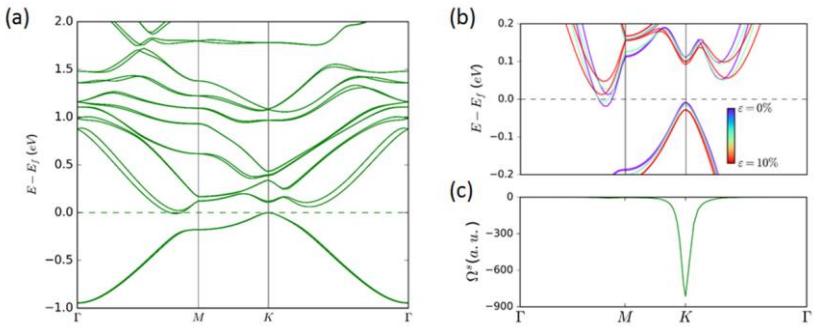

FIG. S4 (a) Electronic band structure of the Au-patterned Ca_2N monolayer with SOC, and (b) evolution of SOC-included band structure under in-plane biaxial strain. (c) The calculated spin Berry curvature along high symmetry paths.

6 Mapping the bands of Ca_2N-Au to the CT lattice model

For pristine Ca_2N monolayer, the DFT calculated band structure shown in FIG.S5 (a)

is consistent with the previous work. The two partially filled parabolic bands, which accommodate the excess electrons, can be fitted nicely by a TB Hamiltonian based on the Ca-s-orbital-like MLWFs, which form two layers of triangular lattices. The inter-layer hopping lifts the band degeneracy. When the Au overlayer is deposited, the evolution of these bands [FIG. S5 (b)] can be modeled by two CT lattices with different hopping parameters, as shown in FIG. S5 (d).

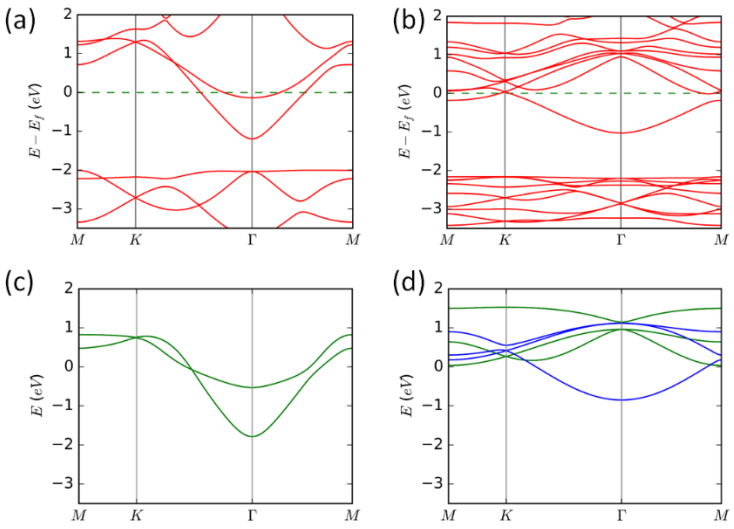

FIG. S5 DFT band structure of Ca_2N monolayer (a) without and (b) with Au overlayer. (c) The parabolic bands fitted by a TB model on two triangular lattices. The NN hopping integral within each layer of triangular lattice is t = -0.21 eV, and the inter-layer NN hopping integral is t' = -0.10 eV (the two bands become degenerate when t'=0). Hoppings are obtained by fitting the DFT bands using the Ca-s-orbital-like MLWFs. (d) TB bands formed by the top (green) and bottom (blue) CT lattice upon deposition of the Au overlayer. The hopping parameters now change for the top CT lattice to t_1= -0.12 eV, t_2 = 0.30 eV (note it becomes positive), and for the bottom CT lattice t_1= -0.23 eV, t_2= -0.18 eV.

7. Topological states in CT lattice from TB model

It is well known that in Kagome lattice the long-range hoppings [8], many-body interactions [9], or spin-orbit coupling (SOC) [10] can perturb the ideal Kagome bands and the system can present topological nontrivial properties. In the CT lattice, if we

consider the periodic patterning potential induced SOC associated with the non-vanishing t_2 hoppings (equivalent to including half of NNN complex hoppings in the conventional Kagome lattice model)

$$H = \sum_{<i,j>} t_1 c_i^{\dagger} c_j + \sum_{<i,j>,\alpha,\beta} c_{i\alpha}^{\dagger} (t_2 - \lambda \sigma_{\alpha\beta}^{z}) c_{j\beta} + h.c. \tag{13}$$

finite gaps will be opened at both Γ and K, as shown in FIG. 2(d) of the main text, which turn out to be topologically nontrivial according to our edge-state and Wannier charge center calculations, as presented in FIG. S6. Inclusion of a Rashba-type SOC (λ_R~8meV estimated from the DFT band splitting, comparable to λ) does not destroy the edges at the 1/3 filling case, as shown in FIG. S7, similar to results studied in [11].

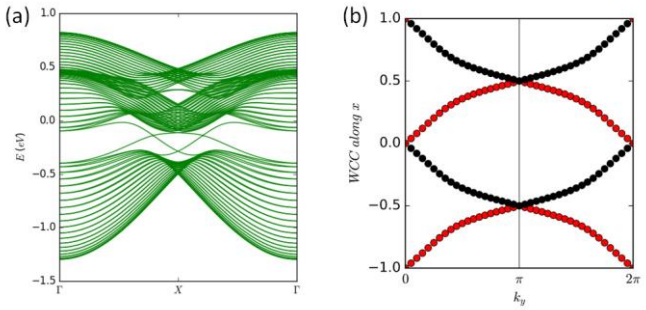

FIG. S6 (a) Edge states and (b) Wannier charge centers (WCC) of CT lattice with SOC.

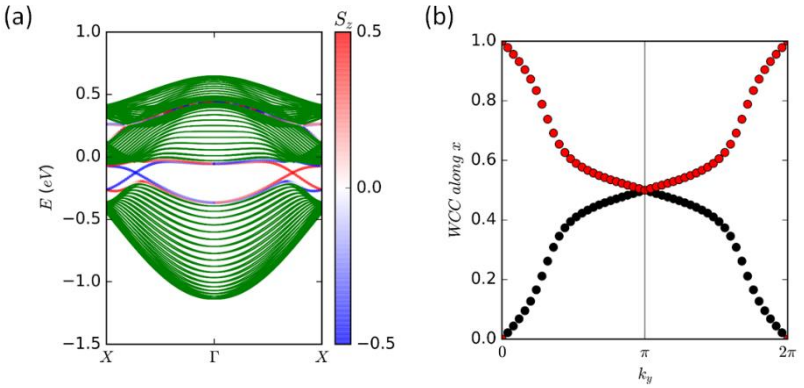

FIG. S7 (a) Topological edge states (spin polarization of the edge states is indicated by different colors) and (b) Wannier charge centers of CT lattice with Rashba SOC.

Supplementary References

[1] S. Alexander and N. Stefan, J. Phys. B **43**, 163001 (2010).

[2] T. Ozawa *et al.*, arXiv preprint arXiv:1802.04173 (2018).

[3] G. Kresse and J. Furthmüller, Phys. Rev. B **54**, 11169 (1996).

[4] P. E. Blöchl, Phys. Rev. B **50**, 17953 (1994).
[5] H. J. Monkhorst and J. D. Pack, Phys. Rev. B **13**, 5188 (1976).
[6] J. P. Perdew, K. Burke, and M. Ernzerhof, Phys. Rev. Lett. **77**, 3865 (1996).
[7] Y. Yao, L. Kleinman, A. H. MacDonald, J. Sinova, T. Jungwirth, D.-s. Wang, E. Wang, and Q. Niu, Phys. Rev. Lett. **92**, 037204 (2004).
[8] H. M. Guo and M. Franz, Phys. Rev. B **80**, 113102 (2009).
[9] W. Zhu, S.-S. Gong, T.-S. Zeng, L. Fu, and D. N. Sheng, Phys. Rev. Lett. **117**, 096402 (2016).
[10] E. Tang, J.-W. Mei, and X.-G. Wen, Phys. Rev. Lett. **106**, 236802 (2011).
[11] Y. Yang, Z. Xu, L. Sheng, B. Wang, D. Y. Xing, and D. N. Sheng, Phys. Rev. Lett. **107**, 066602 (2011).